ACS APPLIED MATERIALS & INTERFACES

Research Article

www.acsami.org

Tailoring the Electrical Properties of HfO_2 MOS-Devices by Aluminum Doping

Albena Paskaleva,*[,†] Mathias Rommel,[‡] Andreas Hutzler,[§] Dencho Spassov,[†] and Anton J. Bauer[‡]

[†]Institute of Solid State Physics, Bulgarian Academy of Sciences, 72 Tzarigradsko Chaussee, 1784 Sofia, Bulgaria

[‡]Fraunhofer Institute for Integrated Systems and Device Technology, Schottkystrasse 10, 91058 Erlangen, Germany

[§]Chair of Electron Devices, Friedrich-Alexander University Erlangen-Nuremberg, Cauerstrasse 6, 91058 Erlangen, Germany

ABSTRACT: In this work dielectric and electrical properties of Al-doped HfO_2 layers deposited by plasma-enhanced atomic layer deposition in dependence on the thickness and the added Al amount in the films have been investigated. Special attention is dedicated to $C-V$ and $I-V$ hysteresis analysis as a measure for trapping phenomena in the films. A detailed study of conduction mechanisms in dependence on the composition of the layers has also been performed. The densities and spatial and energy positions of traps have been examined. It is found that only a small amount of Al-doping decreases the trapping which is assigned to a reduction of oxygen vacancy-related traps in HfO_2. On the contrary, higher amounts of Al introduced in HfO_2 films increase the trapping ability of the stacks which is due to the introduction of deeper Al_2O_3-related traps. The results imply that by adding a proper amount of Al into HfO_2 it is possible to tailor dielectric and electrical properties of high-k layers toward meeting the criteria for particular applications.

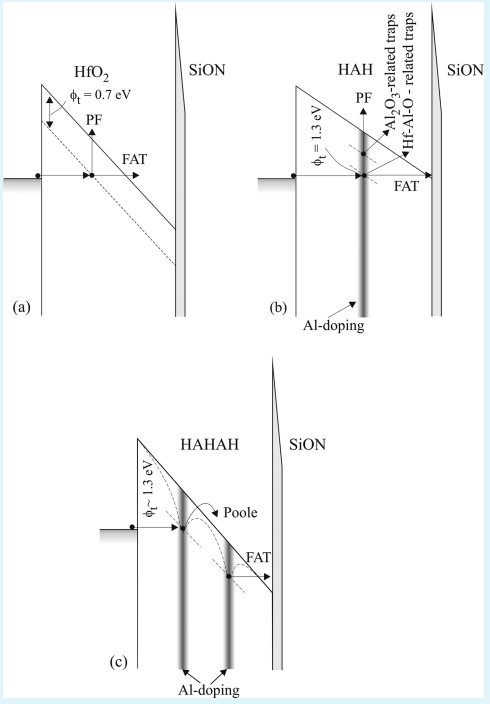

KEYWORDS: *high-k dielectrics, Al-doped HfO_2, trapping, charge trapping memory, conduction mechanisms*

INTRODUCTION

In past years, significant progress has been made in the screening and the selection of high-k gate dielectrics for their integration into current and future CMOS technologies. The intensive studies identified HfO_2 as one of the most promising dielectrics to replace SiO_2 in MOSFET applications. Nevertheless, the successful implementation of HfO_2 as a gate dielectric was hampered by its low temperature of crystallization, thermal instability in contact with Si, and high defect densities which cause threshold voltage instabilities. Increased scattering and degradation of carrier mobility as well as accelerated wear-out and breakdown[1−4] are further issues of concern. Respectively, the possibility to modify physical, electrical, and dielectric properties of HfO_2 layers by doping with different elements or mixing with other dielectrics was considered as a crucial approach toward their implementation as gate dielectrics in MOSFETs. The problems with crystallization and interface quality can be circumvented by alloying the desired oxide with a good glass former—SiO_2 or Al_2O_3—giving either silicate or aluminate.[5−7] This occurs because the dopant atoms (Si, Al, N) distort the originally more ordered structure and thus increase entropy, which suppresses the crystallization process.

The enormous progress in technology and deposition techniques as well as the substantial knowledge acquired on the properties of HfO_2-based high-k dielectrics formed the needed background and opened up new frontiers in considering these dielectrics and their modifications as viable candidates and implementing them in a number of emerging nanoelectronic devices and applications. In particular, Hf-aluminates and $HfO_2-Al_2O_3$ nanolaminates have been investigated for applications as charge storage and blocking oxide layers in charge trapping flash memories;[8,9] interpoly dielectrics in floating gate flash memories;[10] in high voltage

Received: April 14, 2015
Accepted: July 21, 2015
Published: July 21, 2015

DOI: 10.1021/acsami.5b03071
ACS Appl. Mater. Interfaces 2015, 7, 17032−17043

charge storage devices for flat panel displays;[11] as dielectric layers integrated with III−V compound substrates for high electron mobility transistors;[12,13] ferroelectric memories;[14] and resistive switching devices.[15]

One big challenge proves to be the varying demands on the high-k dielectrics for different fields of applications. For example, while charge trapping is strongly undesirable and harmful for the operation of logic CMOS devices, it is of vital importance for some memory devices. In this case the dielectric layers should be engineered in order to obtain high charge trapping efficiency, long retention times, and improved endurance and programming efficiency. The optimization of the fabrication process (method of dielectric deposition and annealing steps) turns out to be very strongly dependent on dielectric material and doping elements used to modify its properties and vice versa—the properties of the films depend strongly on the fabrication technology. In recent years high-k dielectrics have attracted increasing attention as charge storage layers in charge trapping flash (CTF) memories. A comprehensive review on this subject could be found in ref 16. In CTF memories the charges are located at spatially discrete traps distributed in the bandgap of the charge trapping layer, unlike the conventional floating gate memories where charges are stored in the conduction band of the floating gate. Because of this, localized charge storage CTF is considered as one of the most promising memory technologies.[17] Up-to-now silicon-oxide-nitride-oxide-silicon (SONOS) structures with Si_3N_4 acting as a charge storage layer have been mainly used to realize CTF memory.[18,19] High-k dielectric materials have relatively high dielectric constant, large conduction band offsets with Si and tunnel oxide, and high trap densities, which made them a very attractive alternative to supersede the conventional Si_3N_4-based CTF.[17] Respectively, HfO_2-based dielectric stacks have been considered and investigated as charge trapping layers in CTF. You et.al.[20] have found that HfO_2 has better charge trapping efficiency than Si_3N_4 and a 2 nm HfO_2 layer stored almost the same charges as a 7 nm Si_3N_4 layer. Different approaches (e.g., annealing steps, doping or stacking with another dielectric, and so on) have also been suggested to increase the charge storage properties of HfO_2 layers. It has been shown[21] that postdeposition annealing at 1030 °C improves the trapping performance of HfO_2 layers, and this is due to increased diffusion of Al from the blocking Al_2O_3 layer and its incorporation in HfO_2. HfO_2/Al_2O_3 laminated stacks with different numbers and thicknesses of layers have also been investigated as a charge trapping layers for CTF memories.[8,22] The enhancement in memory performance and reliability has been attributed to the modulation of charge distribution by the bandgap engineering of the trapping layer.[8] It has been also reported[22] that increasing the number of the HfO_2/Al_2O_3 interfaces could enhance the charge trapping capability of devices which is due to an interdiffusion at the HfO_2/Al_2O_3 interface that creates additional defects. The thickness of the layers and number of interfaces should be carefully optimized as the electrostatic repulsion between the trapped charges could deteriorate the performance.[23] Despite the intensive investigations, it is still unclear where and how the charges are stored—at interfaces or in the bulk traps; is it necessary to use engineered laminated stacked trapping layers or the required trapping efficiency could be achieved with a single layer high-k dielectric. To answer these questions, more detailed information and deep insight into Al-related traps in HfO_2 should be acquired. In this work, the influence of the concentration of Al-doping on the electrical properties and trapping phenomena in the doped HfO_2 layers deposited by remote plasma-enhanced atomic layer deposition (PE-ALD) is investigated.

EXPERIMENTAL SECTION

Al-doped HfO_2/SiON/p-Si dielectric stacks were grown by PE-ALD. Interfacial SiON layers were deposited by a remote plasma process for 10 s at a plasma power of 400 W using O_2 and N_2 flows of 15 cm^3(STP) min^{-1} each. The resulting thickness of the interfacial layer was about 1.5 nm. After SiON layer formation the pure or Al-doped HfO_2 layers were deposited at a temperature of 300 °C. Tetrakis-(diethylamino)hafnium and Trimethylaluminum were used as Hf and Al precursors, respectively. The O_2 plasma pulse time used for deposition of HfO_2-based dielectric layers was 3 s. Postdeposition annealing (PDA) of all of the samples was performed in O_2 atmosphere at 700 °C for 15 s. Samples with different deposition cycles (i.e., different thicknesses) and different doping were fabricated (Table 1).

Table 1. Composition and Designation of Samples Investigated

designation of sample	HfO_2 (cycles)	Al_2O_3 (cycles)
HfO_2, 50cy	50	
HfO_2, 75cy	75	
HAH(25/5/25)	50	5
HAH(36/2/36)	72	2
HAH(36/5/36)	72	5
HAHAH(24/2/24/2/24)	72	4

The designation of the samples in Table 1 represents the sequence of HfO_2 and Al_2O_3 cycles (cy) used to deposit a given sample (e.g., HAH(36/5/36) represents a sequence of 36 cy of HfO_2, followed by 5 cy of Al_2O_3, and another 36 cy of HfO_2). Since the highest concentration of Al incorporated is only 5 cy of Al_2O_3, it is not likely that a closed layer, showing properties of pure Al_2O_3 like a bandgap, was formed. Therefore, we suggest that it is more proper to consider the films rather as Al-doped HfO_2 than as laminated $HfO_2/Al_2O_3/HfO_2$ structures. The implication of this is that the HAH structures should be regarded as single inhomogeneous layers and not as three-layer structures. To form MOS capacitors, as a top electrode first a 20 nm thick layer of TiN and followed by a thick layer of AlSi were sputter deposited and patterned by photolithography. The area of the capacitors was 4×10^{-4} cm^2. The thicknesses of the HfO_2-based dielectric layers were measured after PDA by a Plasmon SD 2000 ellipsometer and are given in Table 2.

TEM images of 75(72) cy pure and Al-doped HfO_2 layers revealed that they are crystalline after PDA at 700 °C. Electrical characterization of the MOS structures was performed by measuring high-frequency capacitance−voltage (C−V) at 100 kHz and 1 MHz (HP 4277A LCZ meter) and temperature-dependent current−voltage (I−V−T) curves

Table 2. Thickness of High-k Layer (d_{hk}; Ellipsometrically Measured), Equivalent Oxide Thickness (EOT), Effective Permittivity (ε_{eff}; Obtained from C−V Measurements), and Calculated Permittivity of High-k Layer (ε_{hk}) of Different Samples

sample	d_{hk} (nm)	EOT (nm)	ε_{eff}	ε_{hk}
HfO_2, 50cy	7.6	3.07	9.68	15.5
HfO_2, 75cy	10.6	3.57	11.57	17.2
HAH(25/5/25)	7.5	2.66	10.95	19.7
HAH(36/2/36)	9.6	3.22	11.57	18.3
HAH(36/5/36)	9.9	2.94	13.12	22
HAHAH(24/2/24/2/24)	9.7	2.85	13.34	22.6

DOI: 10.1021/acsami.5b03071
ACS Appl. Mater. Interfaces 2015, 7, 17032−17043

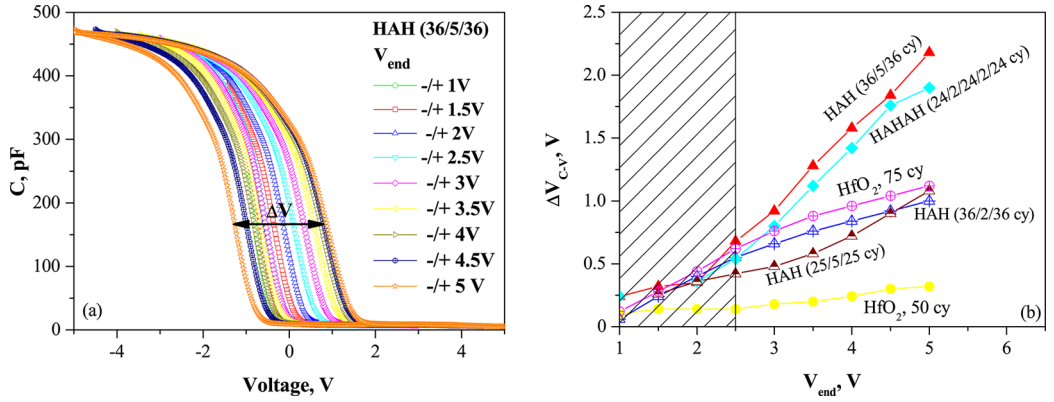

Figure 1. (a) $C-V$ curves of the HAH(36/5/36) sample measured in different voltage ranges ($-V_{end} \rightarrow +V_{end} \rightarrow -V_{end}$). The memory window ΔV_{C-V} is shown. (b) Dependence of memory window ΔV_{C-V} on V_{end} for different samples.

(HP 4156C or HP 4145A semiconductor parameter analyzers). All voltages are given with respect to a grounded substrate.

RESULTS AND DISCUSSION

***C−V* Measurements.** In Table 2 the thickness of the high-k layers measured by ellipsometry (d_{hk}), equivalent oxide thickness (EOT), and effective dielectric constant (ε_{eff}) obtained from $C-V$ measurements as well as calculated permittivity (ε_{hk}) of the HfO_2-based high-k layer are presented. ε_{hk} was calculated by the assumption of a two-layer stack dielectric SiON/high-k, where the thickness and permittivity of the interfacial SiON layer are d_{if} = 1.5 nm and ε_{if} = 5, respectively. Because the composition, thickness, and permittivity of the interfacial layer after deposition of high-k and PDA are not known, the extracted values of ε_{hk} should be considered only as giving a qualitative estimation and the trend of change. In all the cases Al-doping decreases the ellipsometrically measured thickness of the dielectric layer. As all relevant parameters of deposition and annealing processes are identical for pure and Al-doped HfO_2 stacks, the thickness decrease implies that the adding of several cycles of Al during the HfO_2 growth produces more dense films. The incorporation of Al in HfO_2 results also in a substantial decrease of EOT, and the thicker the layer, the larger the EOT decrease is; e.g., for the thinnest (50 cy) sample the decrease is 0.4 nm, while for 100 cy HfO_2 (not shown) it is 0.8 nm. This results in a higher ε_{eff} of Al-doped HfO_2 films compared to their pure counterparts. Eventually, the extracted values of ε_{hk} are also higher; i.e., ε_{hk} = 15−17 for pure HfO_2, whereas for Al-doped films ε_{hk} = 18−22. An increase of the dielectric permittivity of HfO_2 by doping with lower permittivity oxides (e.g., Y_2O_3 and Al_2O_3) was reported also by other authors[24,25] and was explained by a shrinking of the molar volume as the dielectric constant (ε) and the molar volume (V_m) are related through the well-known Clausius−Mossotti equation:

$$\varepsilon = (V_m + 2\alpha/3)/(V_m - \alpha/3) \quad (1)$$

where α is the molecular polarizability. Therefore, a possible explanation is that the incorporation of a small amount of Al in HfO_2 causes some local rearrangements and densifications of the dielectric layers, which results in a smaller molar volume, hence a higher permittivity of the dielectric. The results presented in Table 2 give evidence that EOT decreases progressively with the increase of Al content (at least in the range of the small amounts of Al used here, i.e., 2, 4, or 5 cy). It seems also that it is important how Al is incorporated, and the HAHAH(24/2/24/2/24) sample, where a total of 4 cy Al are incorporated at two positions equidistantly from the two surfaces, produces slightly smaller EOT compared to HAH(36/5/36) where 5 cy of Al is incorporated at one position in the middle of the film.

Next, forward and backward $C-V$ curves were measured for different voltage ranges (i.e., the measurement voltage is changed in the range $-V_{end} \rightarrow +V_{end} \rightarrow -V_{end}$) and the dependence of the $C-V$ hysteresis ΔV_{C-V} on V_{end} is investigated. This dependence is usually used as a measure for the ability of a stack to store a charge, and ΔV_{C-V} is called a memory window. For example, in Figure 1a the $C-V$ curves with increasing V_{end} are given for sample HAH(36/5/36). $\Delta V_{C-V}(V_{end})$ curves obtained at 100 kHz for all stacks are presented in Figure 1b. The following features are clearly visible:

(1) The thickness is a very important parameter influencing strongly the effective charge storage behavior. Thinner samples have smaller memory windows. The thinnest pure HfO_2 reveals a very small hysteresis—it is below 0.15 V for V_{end} up to 2.5 V and increases up to 0.32 V for V_{end} of 5 V. For the 75 cy HfO_2 sample these values are ΔV_{C-V}(2.5V) = 0.6 V and ΔV_{C-V}(5V) = 1.1 V, respectively. Similarly, the hysteresis values of thicker HAH(36/5/36) samples are much larger than those of thinner HAH(25/5/25). It should be noticed that despite the equal doping of the two layers, the trapping in the thicker one is more efficient which is revealed by the larger hysteresis values. The strong thickness dependence implies that the trapping occurs in the bulk of the high-k layer.

(2) Another very important parameter is the level of doping—depending on this level hysteresis could decrease (2 cy Al_2O_3) or increase (4 and 5 cy Al_2O_3); stronger Al-doping increases the quantity of trapped charge; thicker samples with more Al_2O_3 cycles demonstrate larger memory windows.

(3) Hysteresis values for V_{end} up to 2.5 V are very similar for all 72(75) cy HfO_2 samples; i.e., ΔV_{C-V}(2.5V) is 0.55−0.7 V, implying that up to 2.5 V the trapping in thicker stacks is not influenced by Al-doping. On the contrary, trapping in thinner (50 cy HfO_2) stacks depends on the doping level, even at V_{end} < 2.5 V and the doped samples show larger hysteresis.

(4) Substantial differences in the curves of various stacks (Figure1b) occur at $V_{end} \sim$ 2.5 V. There are two types of $\Delta V_{C-V}(V_{end})$ dependencies. For pure HfO_2 samples as well as the sample with the lowest (2 cy) Al-doping the $\Delta V_{C-V}(V_{end})$ curves increase only slightly with increasing V_{end}. For samples

DOI: 10.1021/acsami.5b03071
ACS Appl. Mater. Interfaces 2015, 7, 17032−17043

with 4 and 5 cy of Al_2O_3, hysteresis increases significantly with increasing V_{end}.

(5) ΔV_{C-V} values are very similar for 100 kHz and 1 MHz (not shown); i.e., $\Delta V_{C-V}(V_{end})$ curves seem to be independent of the measurement frequency.

There could be two reasons for the $C-V$ hysteresis:

(1) Because $C-V$ curves are measured in a wide voltage range (−5 to +5 V), the high measurement voltage itself could generate some electrically active defects; i.e., these are stress-induced charges. This process could give rise to irreversible part of $C-V$ hysteresis as it is due to generation of a new (usually permanent) damage in the films).

(2) Trapping in existing traps could contribute to the charge storage; i.e., this is the useful trapping process in the case when the high-k layer is considered as a charge trapping layer in charge trapping flash memories. This process is reversible as the electrons could be trapped and detrapped alternately in these traps under proper biasing conditions.

Thus, we tried to differentiate between the two processes which could give rise to hysteresis and to defining the dominant one of them. For this purpose, two sets of experiments were performed:

(1) $C-V$ curves were measured in the voltage range of (−3 V to V_{end}); i.e., the start voltage was fixed at −3 V, and the stop voltage was varied progressively in the range of (+1 to +5 V). By keeping a small start voltage, any possible effect of high negative voltage stress is minimized and only the effect of high positive voltage stress is studied. Then, the (−3 to +1 V) $C-V$ curve was measured again to establish whether the hysteresis effect is reversible, hence whether the hysteresis is due to positive stress-induced permanent damage or trapping in existing sites. Finally, the (−5 to +5 V) curve was measured.

(2) The $C-V$ curves were measured in the voltage range of (V_{start} to +1 V); i.e., the end voltage was fixed at +1 V and the start voltage was varied progressively in the range of (−3 to −5 V). Respectively, in this case the effect of high negative stress is studied, while minimizing the effect of positive stress. The (−3 to +1 V) $C-V$ curve was measured again, followed by the (−5 to +5 V) curve measurement. These two sets of experiments were performed on pure 75 cy HfO_2 and HAH(36/5/36) samples (Figure 2) as these two samples are representative for the two types of the $\Delta V_{C-V}(V_{end})$ dependencies observed in Figure 1b.

For pure HfO_2 it is seen that by increasing V_{end} the forward $C-V$ curve does not change at all (Figure 2, right-hand side) in the first set of measurements. The backward curves move to more positive voltages, revealing negative charge trapping. This negative charge trapping is most probably due to injection of inversion electrons from the Si substrate and subsequent trapping in HfO_2. It should be noted that hysteresis tends to saturate for $V_{end} \geq 3$ V. The largest hysteresis is about ΔV_{C-V} = 0.9 V. The (−3 to +1 V) curve measured after performing these measurements (half-filled squares in the right-hand side of Figure2) coincides with the initial (−3 to +1 V) curve. This result implies that inversion injection does not create stress-induced damage which may give rise to hysteresis; the trapping is reversible and occurs in existing traps. In the second set of measurements on pure HfO_2 (Figure 2, left-hand side) both the forward and backward $C-V$ curves shift in negative direction and the shift of the forward curves is larger. This implies positive charge trapping. Unlike the first set of measurements, the (−3 to +1 V) curve measured after the (−5 to +1 V) curve (half-filled squares in the left-hand side of Figure 2) is

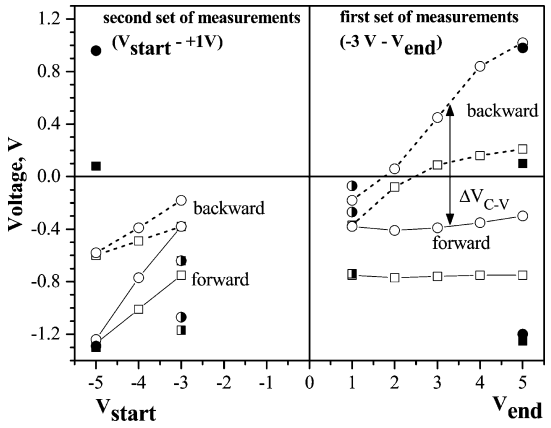

Figure 2. Evolution of $C-V$ voltage shift (open symbols) during (−3 V to V_{end}) measurements (right-hand side) and during (V_{start} to +1 V) measurements (left-hand side). The shift of backward curves (dashed lines) with respect to forward curves (full lines) gives the hysteresis ΔV_{C-V} at given V_{end} or V_{start}. All kinds of squares represent the HfO_2 (72 cy) sample, whereas circles represent the HAH(36/5/36) sample. Semifilled symbols represent the $C-V$ shift for (−3 to +1 V) curve measured after performing measurements with changing V_{end} or V_{start}; filled symbols represent (−5 to +5 V) $C-V$ curve shifts. The voltage shifts are taken with respect to V = 0 V.

significantly shifted with respect to the initial curve and is almost coincident with the (−5 to +1 V) curve; i.e., in this case hysteresis is not reversible and most likely it reflects the stress-induced damage. The hysteresis of the (−5 to +1 V) curve is about ΔV_{C-V} = 0.7 V and we assume that this shift is a measure for the irreversible stress-induced damage in the HfO_2 layer. The more general conclusion is that injection at accumulation generates a positive oxide charge. Therefore, the results obtained reveal that the first set of measurements gives information about the reversible trapping in existing traps, which could be used for charge storage, whereas the second set of measurements reflects the stress-generated damage. In terms of hysteresis values this means that $\Delta V_{C-V} \sim$ 0.9 V is due to electron trapping and $\Delta V_{C-V} \sim$ 0.7 V is due to stress-induced positive charge formation. The sum of the two is ∼1.6 V, which is consistent with the measured hysteresis of ∼1.4 V of the (−5 to +5 V) curve. It should be noted that the hysteresis of (−5 to +5 V) curves for both kinds of measurements is one and the same (full squares in Figure 2).

The two sets of measurements performed on the HAH(36/5/36) sample (Figure 2) show the following: generally, dependencies of ΔV_{C-V} on V_{start} and V_{end} are similar to those obtained in pure HfO_2. Here, we will focus on the differences. The first to be mentioned is that during the first set of measurements ΔV_{C-V} does not saturate and increases progressively with increasing V_{end} and the ΔV_{C-V} obtained for the (−3 to +5 V) $C-V$ curve is ∼1.35 V; i.e., it is significantly larger than that for pure HfO_2. The (−3 to +1 V) curve measured after the (−3 to +5 V) curve is only slightly shifted in the positive direction with respect to the initial curve (half-filled circles in the right-hand side of Figure 2), thus showing that in this case trapping is again reversible and occurs in preexisting traps whose density is larger than that in pure HfO_2. The hysteresis value of the (−5 to +1 V) $C-V$ curve is exactly the same (0.7 V) as that for pure HfO_2; i.e., if we use this value as a measure for stress-induced damage, it can be concluded that Al-doping does not influence the stress-induced positive oxide charge which builds-up in the HfO_2 matrix. It

DOI: 10.1021/acsami.5b03071
ACS Appl. Mater. Interfaces 2015, 7, 17032−17043

should be mentioned that in the case of the HAH sample the hysteresis value in the second set of measurements shows some (albeit small) recovery. The sum of maximal ΔV_{C-V} values obtained in the two sets of measurements is ~2.1 V which is also in agreement with the measured value of ~2.2 V of the (−5 to +5 V) curve. These investigations show that the differences in $C-V$ hysteresis values between pure and Al-doped HfO_2 samples at stop voltages larger than ~2.5 V are due to electron trapping in preexisting Al-related traps; i.e., Al-doping increases the charge storage ability of HfO_2 layers. The smaller hysteresis values for thinner Al-doped oxides with the same amount of doping (HAH(25/5/25) sample) is most probably a result of increased leakage of trapped electrons, which is due to the higher electron tunnelling probability in thinner layers. In other words, the amount of Al-doping may define the number of available traps. The amount of charge trapped in these traps (which gives rise to hysteresis phenomena), however, is dependent not only on the trap density but also on spatial and energy positions of traps. Therefore, in a viewpoint of the charge storage ability of the layers, the high density of traps is not enough. The composition and thickness of layers should be optimized to obtain a proper energy and spatial position of traps and to increase the trapping efficiency. In this context, the HAH(36/5/36) and HAHAH(24/2/24/2/24) samples are most promising, and further we will focus our investigations mainly on these samples to clarify the origin of their better charge storage ability.

***I−V* Measurements.** In Figure 3 the $I-V$ curves of pure and doped 75(72) cy HfO_2 are presented. The pure and lightly doped HAH(36/2/36) samples show similar leakage currents. Also, the two more heavily doped (4 and 5 cy Al_2O_3) samples reveal similar $I-V$ curves. The leakage currents in the latter group of samples are significantly smaller than the leakage currents in the former group. If one compares Figure 3 and Figure 1b, it seems that the larger the memory window is, the smaller the current. This leads us to suggest that the lower leakage current is probably due to the trapping of negative charge, which changes the internal field, hence the current. To prove this, the leakage current values are compared after correcting the applied voltage V_a with the voltage created by the trapped charge, $\Delta V_{C-V}(V_{end}(I-V))$, so that the resultant internal voltage is 1 V; i.e., $V_a - \Delta V_{C-V}(V_{end}(I-V)) = 1$ V. In other words, the current values for different samples are compared at different V_a, which is chosen for each sample to provide an equal internal voltage of 1 V, when corrected with the field created by the trapped charge. The results are presented in Table 3. As is seen with the correction for the field created by the trapped charge, all of the samples reveal similar leakage current density values of ~$(1-2.5) \times 10^{-7}$ A/cm^2 at internal voltage of 1 V. To investigate further the influence of the trapping on $I-V$ characteristics, the following measurements were performed. Three consecutive $I-V$ curves were measured for one polarity and then a set of another three consecutive $I-V$ curves in the opposite polarity. The results for pure 75 cy HfO_2 and HAHAH(24/2/24/2/24) samples are presented in Figure 4a,b. As is seen, there is always a shift ΔV_{I-V} at lower fields when the $I-V$ curve is measured after a measurement in opposite polarity, whereas at higher fields the $I-V$ curves are almost coincident. Consecutive curves measured in one polarity are also coincident. The procedure of alternate positive−negative bias measurements is repeated several times, and the obtained results are very repeatable as seen in Figure 4 (different colors and line styles).

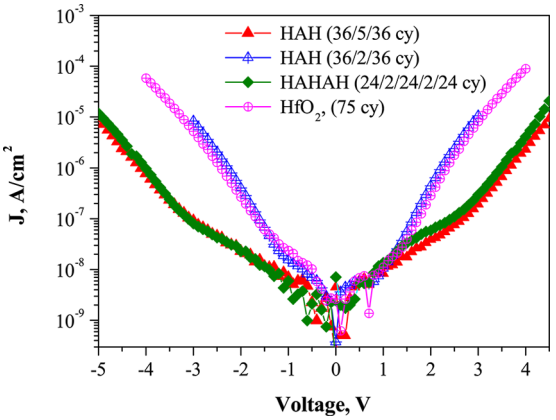

Figure 3. $J-V$ curves of pure HfO_2 and doped with different amounts of Al HfO_2 films with similar thickness.

It is also seen that the HAHAH sample which reveals larger $C-V$ hysteresis shows also larger $I-V$ hysteresis. $C-V$ and $I-V$ hysteresis values for all of the samples are summarized in Table 4 for a measurement temperature of 30 °C. In this table the maximal hysteresis values of $I-V$ curves $\Delta V_{I-V}^{+}(\max)$ and $\Delta V_{I-V}^{-}(\max)$ in positive and negative bias polarity, respectively, are compared with the $C-V$ hysteresis values measured at $V_{end} = \pm 5$ V and at the end voltage of the respective $I-V$ curve measurement, (e.g., for the pure HfO_2 sample it is ±4 V (Figure 4a); for HAHAH it is ±5 V (Figure 4b). A comparison of the results reveals that ΔV_{I-V} values, similarly to ΔV_{C-V} values, are also thickness- and doping-dependent. All dependencies observed for ΔV_{C-V} values keep valid for ΔV_{I-V} values—the thicker layers show larger $I-V$ hysteresis than their respective thinner counterparts; the 4 and 5 cy Al-doped layers exhibit significantly larger shifts than undoped HfO_2 irrespectively of physical thickness; 2 cy Al-doping seems to decrease trapping effects in HfO_2, and in this case the hysteresis is smaller than that of the undoped sample.

As in the case of $C-V$ hysteresis, the thicker layer HAH(36/5/36) reveals larger hysteresis values than the thinner one HAH(25/5/25) with the same amount of Al-doping. This is

Table 3. Comparison of Current Values after Correction of Applied Voltage (+1 V) with That Created by the Trapped Charge ($\Delta V_{C-V}(V_{end}(I-V))$) for Samples under Investigation [$V_{end}(I-V)$, maximal Voltage to Which the $I-V$ Curves Are Scanned; $\Delta V_{C-V}(V_{end}(I-V))$, $C-V$ Hysteresis Measured in a Voltage Range ($-V_{end}(I-V)$ to $+V_{end}(I-V)$]

sample	V_{end} ($I-V$) (volts)	$\Delta V_{C-V}(V_{end}(I-V))$ (volts)	J@+1V+$\Delta V_{C-V}(V_{end}(I-V))$ (A/cm^2)
HfO_2, 75cy	±4	0.96	2.5×10^{-7}
HAH(36/2/36)	±3	0.66	1.3×10^{-7}
HAH(36/5/36)	±4.5	1.85	1.4×10^{-7}
HAHAH(24/2/24/2/24)	±5	1.9	2.3×10^{-7}

DOI: 10.1021/acsami.5b03071
ACS Appl. Mater. Interfaces 2015, 7, 17032−17043

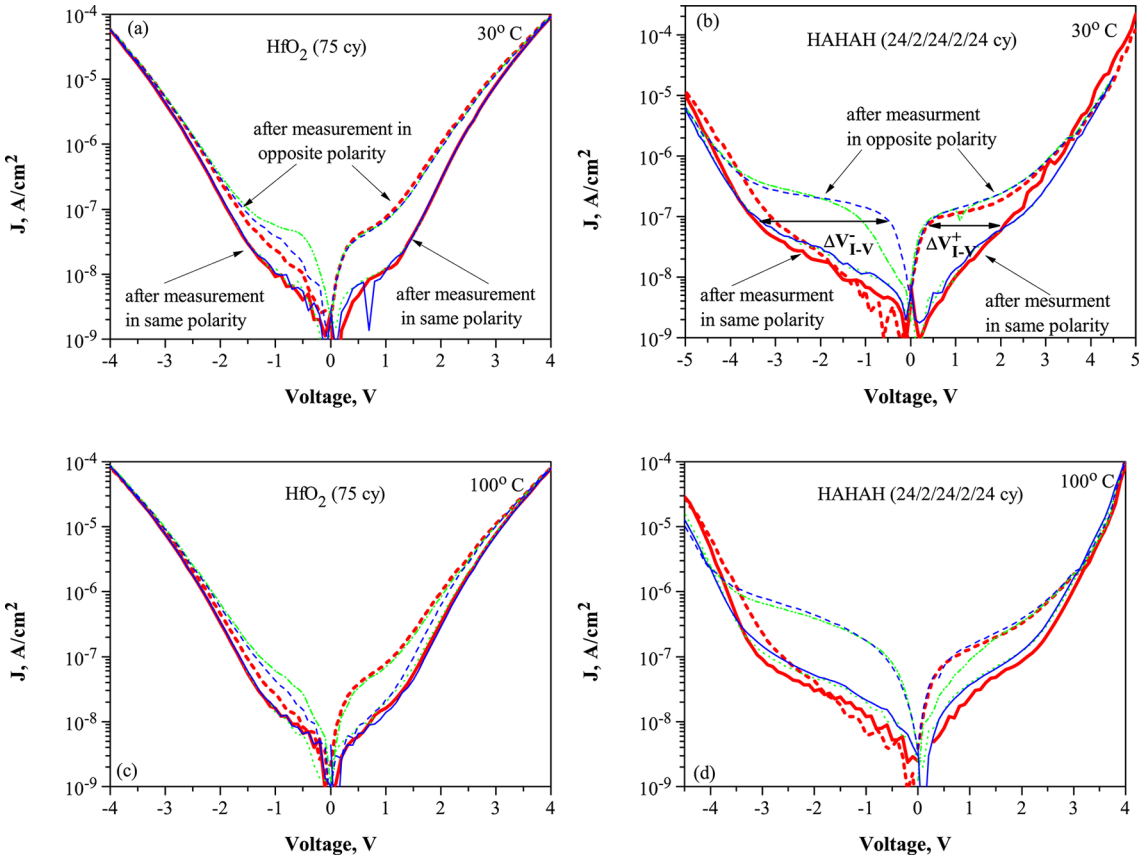

Figure 4. Consecutive $J-V$ measurements in both polarities performed at 30 °C for (a) HfO_2 (75 cy) and (b) HAHAH(24/2/24/2/24) and 100 °C for (c) HfO_2(75cy) and (d) HAHAH(24/2/24/2/24) samples. The curves in different line styles and colors show the reproducibility of trapping/detrapping processes taking place in the structures during repeated measurements.

Table 4. Comparison of the Maximal Hysteresis of $I-V$ Curves Measured at Positive $\Delta V^{+}_{I-V}(\max)$ and Negative $\Delta V^{-}_{I-V}(\max)$ Voltage Polarity and the $C-V$ Curves Hysteresis Values $\Delta V_{C-V}(V_{end}(I-V))$ and $\Delta V_{C-V}(5V)$

sample	$\Delta V^{+}_{I-V}(\max)$	$\Delta V^{-}_{I-V}(\max)$	$\Delta V_{C-V}(V_{end}(I-V))$	$\Delta V_{C-V}(5V)$
HfO_2, 50cy	0.25	0.55	0.15	0.3
HfO_2, 75cy	1	1.1	0.96	1.12
HAH(25/5/25)	1.05	1.6	0.6–0.7	1.1
HAH(36/2/36)	0.4	0.8	0.66	1.0
HAH(36/5/36)	1.85	2.45	1.84	2.18
HAHAH(24/2/24/2/24)	1.8	2.8	1.9	1.9

another confirmation of our suggestion for the more efficient storage of trapped charge in thicker layers. For most of the samples $\Delta V_{C-V}(V_{end}(I-V)) = \Delta V^{+}_{I-V}$. This result and the similar behavior of ΔV_{I-V} and ΔV_{C-V} in dependence on thickness and level of doping imply that they have the same origin. In addition, Table 4 implies that for almost all of the samples (and especially for those exhibiting larger hysteresis), $\Delta V^{-}_{I-V} > \Delta V^{+}_{I-V}$; i.e., hysteresis obtained at gate injection is larger than hysteresis obtained at substrate injection.

The alternate $I-V$ measurements were performed also at 100 °C (Figure 4c,d). It is seen that a hysteresis is also observed at this temperature, and its values are only slightly smaller compared to those obtained at room temperature. We suggest that the hysteresis phenomenon is a result of some kind of equilibrium between trapping and detrapping in the structures. It is well-known that trapping is only slightly temperature-dependent, while detrapping is a strongly temperature-dependent process.[26−28] In this context, the observed weak temperature dependence of the hysteresis implies that trapping/detrapping is performed in relatively deep traps, and an increase in temperature could not provoke increased detrapping.

Conduction Mechanisms. The results presented up-to-now revealed that Al-doping introduces some specific defects which enhance the trapping in HfO_2 layers. The trapped charge is most probably the reason for the reduced leakage current in Al-doped HfO_2 films, and there is evidence that the charge is trapped in relatively deep traps. To get more information and a deeper insight into the trapping phenomena and the spatial and energy distribution of the traps, temperature-dependent $I-V$ measurements were performed (Figure 5) and conduction mechanisms were investigated. As is seen there, are significant differences between the samples, especially at negative biases when the electrons are injected from the gate. In positive polarity (injection from substrate) the leakage current is dominated by the conduction through the interfacial SiON layer which results in temperature behavior similar to that of the $I-V$ curves (for $T < 120$ °C) for all the samples. Therefore,

DOI: 10.1021/acsami.5b03071
ACS Appl. Mater. Interfaces 2015, 7, 17032−17043

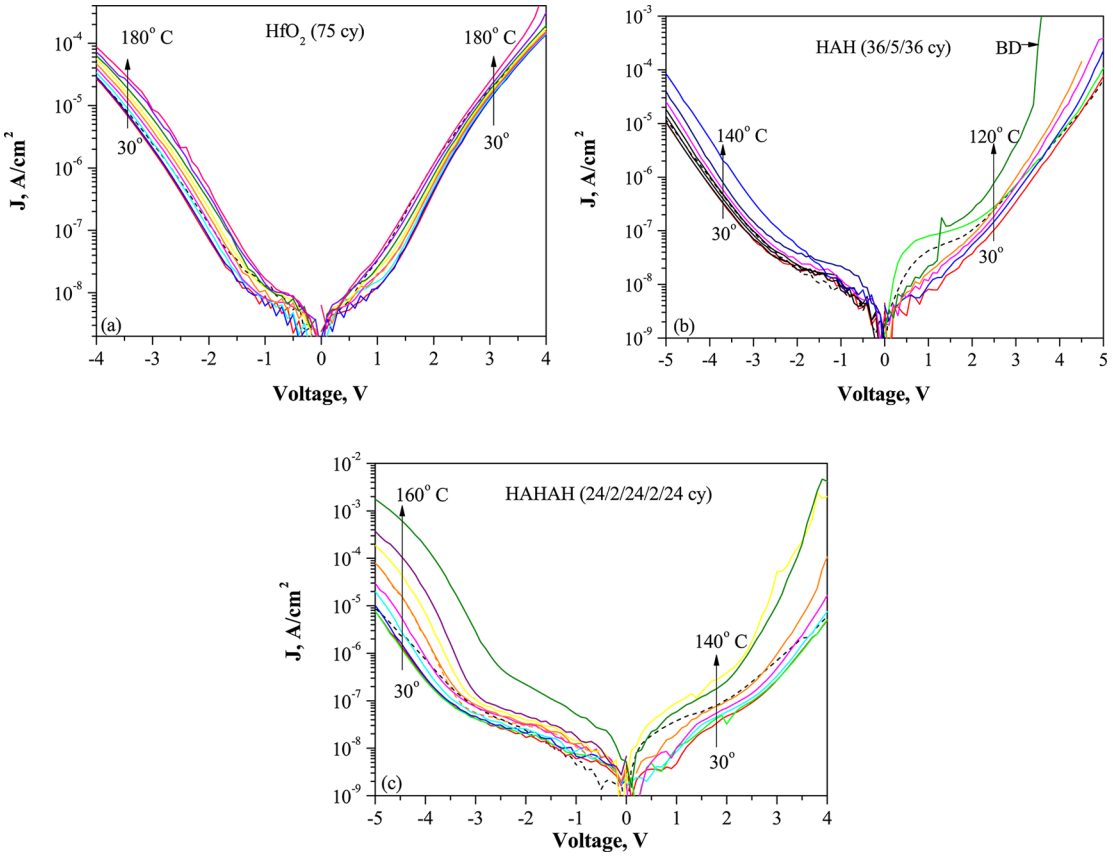

Figure 5. Temperature-dependent $I-V$ measurements for (a) HfO_2(75cy), (b) HAH(36/5/36), and (c) HAHAH(24/2/24/2/24) samples.

we will focus our attention on the behavior of the $I-V$ curves in negative polarity.

When considering the possible conduction mechanisms, the stacked structure of the dielectric layer should be taken into account. The voltage drops across the high-k dielectric—V_{hk}—and across the nitrided interfacial layer—V_{if}—can be obtained by the well-known equations[29]

$$V_{hk} = \frac{V_a}{\frac{\varepsilon_{hk}}{\varepsilon_{if}}\frac{d_{if}}{d_{hk}} + 1} \qquad V_{if} = \frac{V_a}{\frac{\varepsilon_{if}}{\varepsilon_{hk}}\frac{d_{hk}}{d_{if}} + 1} \tag{2}$$

The pure HfO_2 film exhibits a very weak temperature dependence of the $J-V$ curves up to 60 °C (Figure 5a) which implies the domination of some tunnelling processes. As the layers are relatively thick (~10 nm), the probability for direct tunnelling is low. Therefore, we consider Fowler–Nordheim (FN) tunnelling. The representation of the curves measured at different temperatures in FN coordinates (i.e., $\ln(J/E_{hk}^2)$ vs $1/E_{hk}$ with $E_{hk} = V_{hk}/d_{hk}$ being the electric field in the high-k dielectric) gives straight lines for $E_{hk} > 1.5$ MV/cm (Figure 6a), and the obtained barrier heights are in the range of 0.6–0.8 eV, i.e., $\phi_b \sim 0.7$ eV with the assumption that the electron mass in HfO_2 is $0.1m_0$ (m_0, free electron mass).[30] As the barrier height at TiN/HfO_2 is expected to be much higher (~2.6 eV),[31] we conclude that the dominant mechanism is not Fowler–Nordheim tunnelling but field-assisted tunnelling (FAT). FAT is a process in which an electron tunnels from the electrode to traps and then from the traps to the conduction band (CB) of the dielectric. In this case, due to the high enough applied field, the electrons experience a triangular barrier, unlike the case of trap-assisted tunneling (TAT), where the

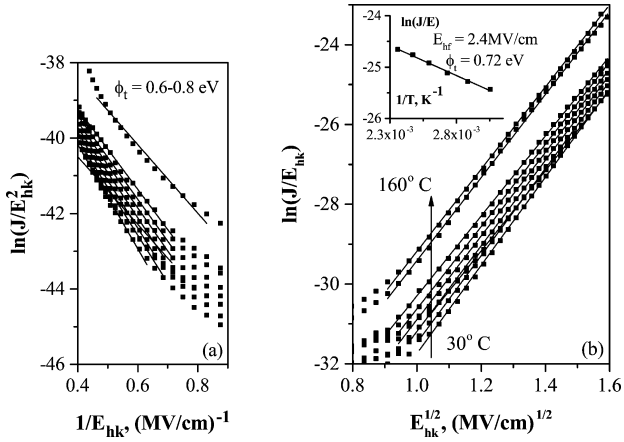

Figure 6. Representation of $I-V$ curves of HfO_2(75cy) sample in (a) Fowler–Nordheim coordinates and (b) Poole–Frenkel coordinates. The inset shows an Arrhenius plot ($\ln(J/E)$ vs $1/T$) at E_{hk} = 2.4 MV/cm and the extracted trap level.

electrons tunnel from the trap to the conduction band of Si not entering the conduction band of the dielectric at all (i.e., in this case they tunnel through a trapezoidal barrier). The equation representing FAT is the same as the FN equation where the barrier height is replaced by the energy position of the traps with respect to the bottom of the conduction band.[32] Therefore, the obtained value of ~0.7 eV is the position of traps (ϕ_t) with respect to the CB of HfO_2. This trap energy corresponds to the energy position of oxygen vacancies in HfO_2, which is reported at ~0.7–0.9 eV.[33,34] The current is temperature-dependent for $T > 60$ °C, which reveals that

DOI: 10.1021/acsami.5b03071
ACS Appl. Mater. Interfaces 2015, 7, 17032–17043

another mechanism also contributes to the conduction. Therefore, we will consider whether Poole−Frenkel (PF) mechanism could operate in the films. The current in the PF mechanism is temperature-dependent and is given by[29,35]

$$J = CE \exp\left(\frac{\phi_t - \sqrt{\frac{q^3E}{\pi\epsilon_0 k_r}}}{rkT}\right) \quad (3)$$

where C is a constant depending on the density of the traps (donor ones) participating in the process and the electron mobility in the insulator conduction band, k_r is the dynamic dielectric constant ($k_r = n^2$, n is the refractive index) and r is a coefficient accounting for the presence of compensating centers (usually acceptor sites; $1 \le r \le 2$). Figure 6b represents the $J-E$ characteristics of the samples in the PF plot ($\ln(J/E)$ vs $E^{1/2}$). As seen for $E_{hk} > 1$ MV/cm, straight line segments are indeed observed. Hence in order to validate the operation of PF mechanism, the obtained value of r^2k_r (from the slope of the line) should be consistent with the refractive index of the dielectric and the limitation $1 \le r \le 2$. Assuming a HfO_2 refractive index of 1.9, the value of k_r is 3.6 and the resultant values of r as obtained from the slope of the line are between 1.5 and 1, showing a temperature dependence as the increase of T reduces the value of r. Therefore, it may be concluded that the current is dominated by the Poole−Frenkel conduction mechanism. The energy position (ϕ_t) of traps participating in PF conduction was extracted from the Arrhenius plot of $I-V$ curves ($\ln(J/E)$ vs $1/T$, inset of Figure 6b). The value of ϕ_t is found to be ∼0.72 eV; i.e., these are the same traps which govern the FAT process at lower temperatures. Therefore, the results imply that the conduction is performed through the traps situated at ∼0.7 eV below the CB of HfO_2. Depending on the measurement conditions (applied voltage and temperature), the dominant conduction mechanism may change. It is worth mentioning that FAT and PF conduction should coexist in principle as they both represent the escape of an electron from a trap and the current is actually a sum of the currents from both mechanisms. The domination of one of them depends on the temperature. FAT dominates at low T, while PF dominates at elevated temperatures.

The HAH(36/5/36) sample exhibits a slightly stronger temperature dependence compared to pure HfO_2 (Figure 5b). Similarly, the current is nearly T-independent up to 60 °C. Therefore, to explain the current conduction in this sample, we have considered the same mechanisms—FAT at $T < 60$ °C and PF at $T > 60$ °C ($E_{hk} > 2$ MV/cm). The same value of k_r (3.6) as in the case of pure HfO_2 was used; i.e., the influence of Al-doping on refractive index is neglected. The obtained r values are between 1.3 and 1, slightly decreasing as T increases from 30 to 160 °C. The fitting gives a trap energy $\phi_t \sim 1.2-1.3$ eV for the FAT process and $\phi_t \sim 0.4-0.5$ eV for the PF process (Figure 7). In other words, unlike the pure HfO_2, in the HAH(36/5/36) sample the FAT and PF processes are mediated by two different trap levels. These results give evidence that Al-doping introduces deeper trap levels than these in pure HfO_2, thus leading to substantial changes in the leakage current levels and the trapping properties of the layers. Further considerations of the conduction mechanisms in the HAHAH(24/2/24/2/24) sample confirm this conclusion and reveal that the way of Al incorporation into HfO_2 is also of substantial importance. For this sample the strongest temperature dependence of the current is observed (Figure 5c). There is still a weak T-dependence up to 60 °C, and above 60 °C the current increases more strongly compared to the HAH(36/5/36) sample. With consideration of the FAT process as a dominant conduction mechanism at $T < 60$ °C, $E_{hk} > 1.4$ MV/cm gives a trap level $\phi_t \sim 1.4$ eV, i.e., slightly deeper than that obtained for the HAH(36/5/36) sample. It should be noted that at $T = 60-120$ °C the curves are also well-fitted by the FAT process and the obtained trap energy is the same (i.e., ∼1.4 eV). However, FAT is nearly temperature-independent, which could not explain the strong temperature dependence observed at $T > 60$ °C. Therefore, it is suggested that FAT is still present at $T > 60$ °C, but some T-dependent process also participates to the conduction. The Poole−Frenkel process does not fit the $I-V$ curves well even at very high temperatures ($T > 120$ °C), and the obtained value for r^2k_r is not consistent with the refractive index (i.e., $k_r = n^2$) and the limitation $1 \le r \le 2$. Therefore, PF is excluded as a possible mechanism explaining current conduction at high temperatures and high fields. Having in mind the peculiarity of the doping process of the HAHAH(24/2/24/2/24) sample, we suggest that in this case the conduction could be governed by Poole conduction, i.e., field-enhanced thermally excited electron hopping between ionized centers with a density high enough to induce overlap in the Coulombic fields between two adjacent sites. In the case of Poole conduction the current obeys the equation[36]

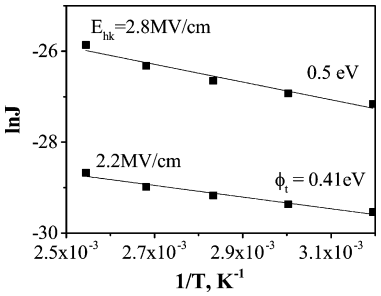

Figure 7. Arrhenius plot ln J vs $1/T$ at two fields of E_{hk} = 2.2 and 2.8 MV/cm and the extracted trap levels for the HAH(36/5/36) sample.

$$J = C_p \exp\left(-\frac{\phi_t - s_p E_{hk}}{kT}\right); \quad s_p = qd_t/2 \quad (4)$$

where d_t is a distance between two ionized centers. A distinct difference between the Poole effect and Poole−Frenkel emission emerges from different densities of ionized centers. Due to a lower density of ionized centers for the PF emission, the Coulombic field between two adjacent sites does not overlap and the ionization barrier lowering for PF emission is affected only by the applied electric field, so that the current obeys the exponential dependence on the root square of the electric field (see eq 3). For Poole hopping, the Coulombic field between the adjacent sites overlaps, which leads to a further decrease in their ionization barrier. As a result, the leakage current obeys the simple exponential dependence on the electric field.[36] Indeed, the Poole conduction fits well the current at $T \ge 100$ °C (Figure 8a). An Arrhenius plot of the current (Figure 8b) reveals that the activation energy of the process controlling leakage current is $E_a \sim 0.2-0.3$ eV for $T < 100$ °C, while at $T \ge 100$ °C a larger activation energy of $E_a \sim 0.6-0.7$ eV is observed. As mentioned previously at $T \ge 100$ °C the Poole conduction controls the current and $E_a = \phi_t - s_pE_{hk}$; i.e., the activation energy is linearly dependent on E_{hk},

DOI: 10.1021/acsami.5b03071
ACS Appl. Mater. Interfaces 2015, 7, 17032−17043

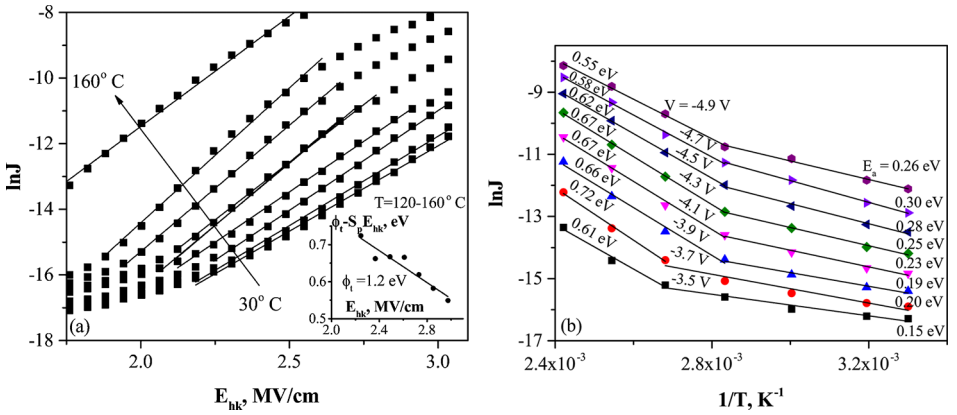

Figure 8. (a) Representation of $I-V$ curves in Poole coordinates (ln J vs E_{hk}) of the HAHAH sample. The inset shows the dependence of activation energy $E_a = \phi_t - s_pE_{hk}$ of Poole conduction on the electric field. (b) Arrhenius plot of the current in HAHAH sample in the whole temperature range (30−100 °C) and for different applied voltages.

and the intercept of the line with the y-axis should give ϕ_t (Figure 8a). In our case, for ϕ_t a value of 1.2 eV is obtained, i.e., very similar to the trap level which controls the FAT process at lower temperatures both in the HAH(36/5/36) and the HAHAH(24/2/24/2/24) samples. This result supports the conclusion that the 1.2 eV level is related to Al-doping. Therefore, the results obtained for this sample reveal that FAT is dominant at T < 60 °C; at 60 °C < T < 100 °C both FAT and Poole conduction are present. With increasing temperature the contribution of Poole conduction increases and at T > 100 °C it is the main mechanism which governs the current in the HAHAH(24/2/24/2/24) sample. The specific way of Al incorporation in the HAHAH(24/2/24/2/24) sample results in a more homogeneous distribution of traps and favors Poole conduction between them.

The conduction mechanisms considered up-to-now dominate at relatively high fields, E_{hk} > 1.5 MV/cm. As is seen in Figure 5c there is a wide electrical field region (V < |−3| V, E_{hk} < 1.3 MV/cm), where the current increases only slightly with applied voltage and temperature. It is exactly the region where the hysteresis of the $I-V$ curves is observed (Figure 4). As already mentioned, this hysteresis is most probably due to the existence of localized traps which change their charge state when a bias with opposite polarity is applied. Therefore, the reasonable suggestion is that in this region the conduction is governed by a space charge limited current (SCLC) mechanism.[37] In the case of a discrete trap distribution, the current governed by SCL mechanism should be proportional to V^2,[37] i.e.,

$$J \propto V^2/d_{hk}^3 \quad (5)$$

and a representation of $I-V$ curves in log−log scale should give a line with a slope of ∼2. This is indeed observed in Figure 9 where $J-E$ curves are presented in log−log plot for the entire applied electric field range. According to the SCLC theory, in the presence of shallow traps (here the term shallow means that the trap is above the Fermi level) (log J)−(log E) curves first should have a slope ∼1, corresponding to Ohmic conduction. As the density of the injected electrons into the insulator exceeds the thermal equilibrium electron concentration (at voltage V_x), the slope of log J vs log E increases to 2, which is observed indeed (Figure 9). V_{TFL} in Figure 9 is a trap-filled limit at which all of the traps are filled. Therefore, in this field

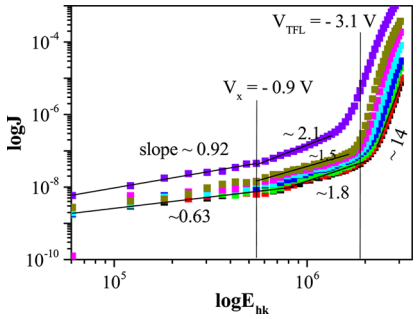

Figure 9. log J vs log E_{hk} curves representing the space-charge-limited conduction at low fields in HAHAH sample.

range SCLC is the dominant mechanism in the HAHAH(24/2/24/2/24) sample.

A schematic representation of the conduction mechanisms and trap levels observed in the different samples in line with the Al-doping profile is shown in Figure 10. In summary, the detailed characterization of conduction mechanisms in different stacks revealed the existence of traps with an energy level of 0.7 eV below the conduction band in pure HfO_2 (Figure 10a) which is consistent with the energy of an oxygen vacancy in HfO_2. The conduction in HfO_2 is performed via these traps, and the dominant conduction mechanism (FAT or PF emission) is defined by the measurement conditions (applied voltage and temperature). Similar results were observed in our previous studies of other dielectrics.[38] In all Al-doped samples the existence of a deeper level (1.2−1.4 eV below the conduction band) is undoubtedly revealed (Figure 10b,c). The 0.7 eV level is not observed at all, while the HAH (36/5/36) sample exhibits an additional trap level at about 0.4−0.5 eV below the conduction band (Figure 10b). The disappearance of the 0.7 eV trap level could be explained by a reduction of the concentration of oxygen vacancies in HfO_2 by Al-doping, which was observed also by other authors.[39] It is also supported by the decreased trapping in the stacks with the lowest Al-doping—HAH(36/2/36) (Figure 1). The increase of Al-doping obviously results in the formation of deeper traps, which have been observed also by Molas et al.,[10] who found a trap level at about 1.35 eV below the conduction band for HfAlO layers with Hf:Al(9:1) and at about 1.55 eV for Hf:Al(1:9). Therefore, we could conclude that the deep level is related to the Al incorporation into HfO_2. Most probably this level is due to

DOI: 10.1021/acsami.5b03071
ACS Appl. Mater. Interfaces 2015, 7, 17032−17043

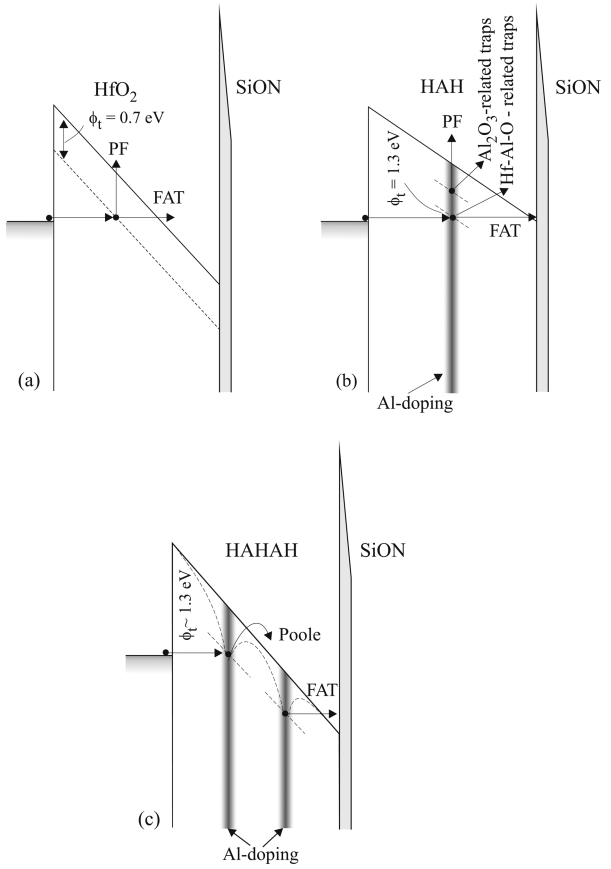

Figure 10. Schematic representation of the dominant conduction mechanisms and trap levels in different samples: (a) HfO_2(75cy); (b) HAH(36/5/36); (c) HAHAH(24/2/24/2/24).

Hf−Al−O bonds (Figure 10b,c) assigned to AlO^- bonding groups deriving from a breaking of the network component, and to antibonding Hf atom d-states that form the lowest conduction band of the alloy.[10] The existence of a 0.4−0.5 eV level in the HAH(36/5/36) sample could be explained by taking into account the difference in the doping approach between this sample and the HAHAH(24/2/24/2/24) sample. As mentioned in ref 40, Al is too small to be effectively incorporated into the fluorite lattice and the solubility of Al in all ZrO_2/HfO_2 phases is relatively low leading to a segregation of Al_2O_3 to form separate Al_2O_3 phases (Figure 10b). We suggest that the process of Al_2O_3 segregation is increased in the HAH(36/5/36) sample where the whole amount of Al is incorporated at one place. Introduction of smaller amounts of Al at two different places allows for more effective incorporation of Al into HfO_2 without segregation into Al_2O_3. This interpretation of results is supported by the observed[41] trap level of about 0.42−0.44 eV in Al_2O_3. It is also coherent with the slightly lower permittivity of the HAH(36/5/36) sample compared to HAHAH. As is well-known the permittivity of Al_2O_3 is about 10 and its inclusion in higher permittivity oxides should result in a layer with reduced permittivity.

Density of Traps. In this section we try to estimate the density of the trapped charge N_t and to obtain some information about its spatial distribution. First, the values of the memory window ΔV_{C-V}(5V) are used to assess N_t. In metal-oxide-high-k dielectric-oxide-Si (MOHOS) structures, which are used for charge storage in charge trapping flash memories, the memory window is proportional to the spatial homogeneously trapped charge density (N_t; cm^{-3}) and could be calculated by using the following equation:[42,43]

$$\Delta V_{C-V} = \frac{qN_t d_{hk}}{\varepsilon_{OB}}\left(d_{OB} + \frac{\varepsilon_{OB} d_{hk}}{2\varepsilon_{hk}}\right) \quad (6a)$$

where d_{OB} and ε_{OB} are the thickness and the dielectric constant of the blocking oxide in MOHOS, respectively. As in our structures there is not any blocking oxide, i.e., $d_{OB} = 0$; the equation transforms to

$$\Delta V_{C-V} = \frac{qN_t {d_{hk}}^2}{2\varepsilon_{hk}} \quad (6b)$$

Another approach to obtain the density of trapped charge is by using the hysteresis values of $I-V$ curves in both polarities. In this case not only N_t but also the centroid of the trapped charge ($\bar{x}$) could be estimated by the following equations:[44]

$$Q_t = \frac{\varepsilon(\Delta V^-_{I-V} - \Delta V^+_{I-V})}{d} \quad (7a)$$

$$\bar{x} = d\left(1 - \frac{\Delta V^-_{I-V}}{\Delta V^+_{I-V}}\right)^{-1} \quad (7b)$$

From Q_t (cm^{-2}), $N_t = Q_t/d_{hk}$ is obtained. The values obtained by the two methods for different samples are summarized in Table 5. As it is seen both methods reveal a larger density of trapped charge in more heavily doped (4 and 5 cy Al) HfO_2 layers—about twice the trap density in pure and 2 cy Al-doped samples. It is seen that the extracted values of N_t from $C-V$ hysteresis are 2× larger than those obtained from $I-V$ hysteresis.

Table 5. Values of the Trapped Charge Densities and Charge Centroid $\bar{x}$ Estimated from $C-V$ and $I-V$ Hysteresis Measurements

sample	$N_t \times 10^{19}(C-V)$ (cm^{-3})	$N_t \times 10^{19}(I-V)$ (cm^{-3})	$\bar{x}$ (nm)
HfO_2, 75cy	1.9	1	6
HAH(25/5/25)	4.3	2.0	3.6
HAH(36/2/36)	2.2	0.6	3.7
HAH(36/5/36)	5.5	2.7	4.95
HAHAH(24/2/24/2/24)	5	3	4.4

We suggest that this is due to the existence of the irreversible part in ΔV_{C-V}; i.e., both trapped charge and stress generated charge contribute to N_t in this case. For pure HfO_2 the centroid is at about 6 nm, i.e., a little closer to the HfO_2/SiON interface, which implies a slightly inhomogeneous distribution of traps. The centroid of the charge for HAH(36/5/36) and HAH(25/5/25) samples is estimated at 4.95 and 3.6 nm, respectively, i.e., just in the middle of the high-k film. This result is consistent with the position of Al-doping in these films and gives evidence that the trapped charge is located in Al-related traps. For the HAHAH sample the obtained centroid at 4.4 nm (i.e., a little closer to the metal interface) may be related to some migration of the Al-dopant toward the top electrode. For the HAH(36/2/36) sample the values of the trapped charge density and the centroid of this charge suffer from significant error and are not very reliable, because of the small values of the $I-V$ hysteresis shifts.

DOI: 10.1021/acsami.5b03071
ACS Appl. Mater. Interfaces 2015, 7, 17032−17043

Finally, the domination of SCL conduction at low fields gives another possibility to assess the trap density. According to SCLC theory,[37] the trap-filled limit V_{TFL} (Figure 9) is related to the trap concentration N_t by

$$V_{TFL}^{hk} \approx \frac{qN_t d_{hk}^{\ 2}}{\varepsilon_{hk}} \quad (8)$$

Having in mind that for the HAHAH sample V_{TFL} is about 3.1 V, the voltage drop across the high-k layer is calculated by using eq 2, and the density of traps is estimated to be $N_t \sim 2.4 \times 10^{19}$ cm^{-3}; i.e., it is in accordance with the value obtained by the $I-V$ hysteresis values.

CONCLUSION

In conclusion, the Al-doping of HfO_2 layers has a strong influence on the trapping phenomena in TiN/Al-doped HfO_2/SiON/Si structures. The dedicated $C-V$ and $I-V$ hysteresis measurements and analysis reveal that the amount of doping as well as the doping approach define to a great extent the trap parameters (e.g., density and spatial and energy location). A small amount of Al-doping results in smaller hysteresis effects with respect to pure HfO_2 layers implying a reduced density of traps. Stronger trapping effects are observed in samples with larger Al-doping. The results give evidence that there are two kinds of traps giving rise to a $C-V$ memory window—stress-induced traps, whose density is independent of Al-doping, which can be related to weak bonds in HfO_2 and Al-related traps which can trap and detrap charge reversibly and hence can be used for charge storage. The detailed conduction mechanisms analysis revealed that the increased charge storage ability of Al-doped HfO_2 is due to the existence of deep Al-related traps with an energy level of 1.2−1.4 eV below the conduction band edge of the dielectric. The 0.7 eV trap level found in pure HfO_2 which is consistent with the energy position of an oxygen vacancy in HfO_2 is not observed in the doped samples. Therefore, Al-doping has two effects on the trap density—it decreases the oxygen vacancy-related defects in HfO_2 and introduces deep traps. The doping level should be carefully optimized to obtain the desired properties of the dielectric layer (e.g., layers with reduced electrically active defects or layers with increased trapping ability) suitable for the particular application. Samples with higher Al-doping reveal a trap density of about $(2-3) \times 10^{19}$ cm^{-3}. The values obtained for the centroid of the trapped charge give further evidence that these are Al-related traps. Al-doping (in the range of small amounts used in this study) decreases also the EOT of the layers, hence increasing the effective dielectric constant of the stack. The larger permittivity values of Al-doped HfO_2 layers with respect to their pure counterparts are most probably due to an Al-induced densification of the layers.

AUTHOR INFORMATION

Corresponding Author

*E-mail: paskaleva@issp.bas.bg.

Notes

The authors declare no competing financial interest.

REFERENCES

(1) Houssa, M.; Pantisano, L.; Ragnarsson, L.Å.; Degraeve, R.; Schram, T.; Pourtois, G.; De Gendt, S.; Groeseneken, G.; Heyns, M. M. Electrical Properties of High-*k* Gate Dielectrics: Challenges, Current Issues, and Possible Solutions. *Mater. Sci. Eng., R* **2006**, *51*, 37−85.

(2) Duschl, R.; Kerber, M.; Avellan, A.; Jakschik, S.; Schroeder, U.; Kudelka, S. Reliability Aspects of Hf-based Capacitors: Breakdown and Trapping Effects. *Microelectron. Reliab.* **2007**, *47*, 497−500.

(3) Zafar, S.; Kumar, A.; Gusev, E.; Cartier, E. Threshold Voltage Instabilities in High-*k* Gate Dielectric Stacks. *IEEE Trans. Device Mater. Reliab.* **2005**, *5*, 45−64.

(4) Choi, J. H.; Mao, Y.; Chang, J. P. Development of Hafnium Based High-*k* Materials—A Review. *Mater. Sci. Eng., R* **2011**, *72*, 97−136.

(5) Wilk, G. D.; Wallace, R.; Anthony, J. M. High-*k* Gate Dielectrics: Current Status and Materials Properties Considerations. *J. Appl. Phys.* **2001**, *89*, 5243−5275.

(6) Manchanda, L.; Morris, M. D.; Green, M. L.; van Dover, R. B.; Klemens, F.; Sorsch, T. W.; Silverman, P. J.; Wilk, G.; Busch, B.; Aravamudhan, S. Multi-Component High-*k* Gate Dielectrics for the Silicon Industry. *Microelectron. Eng.* **2001**, *59*, 351−359.

(7) Zhu, W. J.; Tamagawa, T.; Gibson, M.; Furukawa, T.; Ma, T. P. Effect of Al Inclusion in HfO_2 on the Physical and Electrical Properties of the Dielectrics. *IEEE Electron Device Lett.* **2002**, *23*, 649−651.

(8) Zhu, C.; Huo, Z.; Xu, Z.; Zhang, M.; Wang, Q.; Liu, J.; Long, S.; Liu, M. Performance Enhancement of Multilevel Cell Nonvolatile Memory by Using a Bandgap Engineered High-*k* Trapping Layer. *Appl. Phys. Lett.* **2010**, *97*, 253503-1−253503-3.

(9) Tan, Y. N.; Chim, W. K.; Choi, W. K.; Joo, M. S.; Cho, B. J. Hafnium Aluminum Oxide as Charge Storage and Blocking-Oxide Layers in SONOS-Type Nonvolatile Memory for High-Speed Operation. *IEEE Trans. Electron Devices* **2006**, *53*, 654−662.

(10) Molas, G.; Bocquet, M.; Buckley, J.; Grampeix, H.; Gély, M.; Colonna, J.-P.; Licitra, C.; Rochat, N.; Veyront, T.; Garros, X.; Martin, F.; Brianceau, P.; Vidal, V.; Bongiorno, C.; Lombardo, S.; De Salvo, B.; Deleonibus, S. Investigation of Hafnium-Aluminate Alloys in View of Integration as Interpoly Dielectrics of Future Flash Memories. *Solid-State Electron.* **2007**, *51*, 1540−1546.

(11) Yoo, Y. W.; Jeon, W.; Lee, W.; An, C. H.; Kim, S. K.; Hwang, C. S. Structure and Electrical Properties of Al-Doped HfO_2 and ZrO_2 Films Grown via Atomic Layer Deposition on Mo Electrodes. *ACS Appl. Mater. Interfaces* **2014**, *6*, 22474−22482.

(12) An, C. H.; Mahata, C.; Byun, Y. C.; Kim, H. Atomic-Layer-Deposited $(HfO_2)_{1-x}(Al_2O_3)_x$ Nanolaminate Films on InP with Different Al_2O_3 Contents. *J. Phys. D: Appl. Phys.* **2013**, *46*, 275301-1−275301-6.

(13) Byun, Y. C.; Mahata, C.; An, C. H.; Kim, H. Starting Layer Dependence of the Atomic-Layer-Deposited $HfAlO_x$ Films on GaAs. *Semicond. Sci. Technol.* **2012**, *27*, 105026−1−105026−4.

(14) Schroeder, U.; Yurchuk, E.; Müller, J.; Martin, D.; Schenk, T.; Polakowski, P.; Adelmann, C.; Popovici, M. L.; Kalinin, S. V.; Mikolajick, T. Impact of Different Dopants on the Switching Properties of Ferroelectric Hafniumoxide. *Jpn. J. Appl. Phys.* **2014**, *53*, 08LE02-1−08LE02-5.

(15) Zhou, P.; Ye, L.; Sun, Q. Q.; Chen, L.; Ding, S. J.; Jiang, A. Q.; Zhang, D. W. The Temperature Dependence in Nanoresistive Switching of HfAlO. *IEEE Trans. Nanotechnol.* **2012**, *11*, 1059−1062.

(16) Zhao, C.; Zhao, C. Z.; Taylor, St.; Chalker, P. R. Review on Non-Volatile Memory with High-*k* Dielectrics: Flash for Generation Beyond 32 nm. *Materials* **2014**, *7*, 5117−5145.

(17) Park, G. H.; Cho, W. J. Reliability of Modified Tunneling Barriers for High Performance Nonvolatile Charge Trap Flash Memory Application. *Appl. Phys. Lett.* **2010**, *96*, 043503-1−043503-3.

(18) Bu, J.; White, M. Design Considerations in Scaled SONOS Nonvolatile Memory Devices. *Solid-State Electron.* **2001**, *45*, 113−120.

(19) Chau, R.; Doyle, B.; Datta, S.; Kavalieros, J.; Zhang, K. Integrated Nanoelectronics for the Future. *Nat. Mater.* **2007**, *6*, 810−812.

(20) You, H. W.; Cho, W. J. Charge Trapping Properties of the HfO_2 Layer with Various Thicknesses for Charge Trap Flash Memory Applications. *Appl. Phys. Lett.* **2010**, *96*, 093506-1−093506-3.

(21) Spiga, S.; Driussi, F.; Lamperti, A.; Congedo, G.; Salicio, O. Effects of Thermal Treatments on the Trapping Properties of HfO_2

DOI: 10.1021/acsami.5b03071
ACS Appl. Mater. Interfaces 2015, 7, 17032−17043

Films for Charge Trap Memories. *Appl. Phys. Express* **2012**, *5*, 021102-1−021102-3.
(22) Lan, X.; Ou, X.; Cao, Y.; Tang, S.; Gong, C.; Xu, B.; Xia, Y.; Yin, J.; Li, A.; Yan, F.; Liu, Z. The Effect of Thermal Treatment Induced Inter-Diffusion at the Interfaces on the Charge Trapping Performance of HfO_2/Al_2O_3 Nanolaminate-Based Memory Devices. *J. Appl. Phys.* **2013**, *114*, 044104-1−044104-7.
(23) Tang, Z.; Zhu, X.; Xu, H.; Xia, Y.; Yin, J.; Liu, Z.; Li, A.; Yan, F. Impact of the Interfaces in the Charge Trap Layer on the Storage Characteristics of ZrO_2/Al_2O_3 Nanolaminate-Based Charge Trap Flash Memory Cells. *Mater. Lett.* **2013**, *92*, 21−24.
(24) Kita, K.; Kyuno, K.; Toriumi, A. Permittivity Increase of Yttrium-Doped HfO_2 through Structural Phase Transformation. *Appl. Phys. Lett.* **2005**, *86*, 102906-1−102906-3.
(25) Park, P. K.; Kang, S. W. Enhancement of Dielectric Constant in HfO_2 Thin Films by the Addition of Al_2O_3. *Appl. Phys. Lett.* **2006**, *89*, 192905-1−192905-3.
(26) Kalpat, S.; Tseng, H.-H.; Ramon, M.; Moosa, M.; Tekleab, D.; Tobin, P. J.; Gilmer, D. C.; Hedge, R. I.; Capasso, C.; Tracy, C.; White, B. E., Jr BTI Characteristics and Mechanisms of Metal Gated HfO_2 Films with Enhanced Interface/Bulk Process Treatments. *IEEE Trans. Device Mater. Reliab.* **2005**, *5*, 26−35.
(27) Luna-Sánchez, R. M.; González-Martinez, I. Charge Trapping in High-k Gate Dielectrics: A Recent Understanding. *ECS Trans.* **2006**, *2*, 311−328.
(28) Aoulaiche, M.; Houssa, M.; Degraeve, R.; Groeseneken, G.; DeGendt, S.; Heyns, M. M. Polarity Dependence of Bias Temperature Instabilities in $Hf_xSi_{1-x}ON$/TaN Gate Stacks. *Proc. 35th European Solid State Dev. Res. Conf. ESSDERC 200. Grenoble, France* **2005**, 197−200.
(29) Chaneliere, C.; Autran, J. L.; Devine, R. A. B.; Balland, B. Tantalum Pentoxide (Ta_2O_5) Thin Films for Advanced Dielectric Applications. *Mater. Sci. Eng., R* **1998**, *22*, 269−322.
(30) Zhu, W. J.; Ma, T.-P.; Tamagawa, T.; Kim, J.; Di, Y. Current Transport in Metal/Hafnium Oxide/Silicon Structure. *IEEE Electron Device Lett.* **2002**, *23*, 97−99.
(31) Afanas'ev, V. V.; Stesmans, A.; Pantisano, L.; Cimino, S.; Adelmann, C.; Goux, L.; Chen, Y. Y.; Kittl, J. A.; Wouters, D.; Jurczak, M. TiN_x/HfO_2 Interface Dipole Induced by Oxygen Scavenging. *Appl. Phys. Lett.* **2011**, *98*, 132901-1−132901-3.
(32) Paskaleva, A.; Bauer, A. J.; Lemberger, M.; Zürcher, S. Different Current Conduction Mechanisms through Thin High-*k* $Hf_xTi_ySi_zO$ Films Due to the Varying Hf to Ti Ratio. *J. Appl. Phys.* **2004**, *95*, 5583−5590.
(33) Gavartin, J. L.; Muñoz Ramo, D.; Shluger, A. L.; Bersuker, G.; Lee, B. H. Negative Oxygen Vacancies in HfO_2 as Charge Traps in High-*k* Stacks. *Appl. Phys. Lett.* **2006**, *89*, 082908-1−082908-3.
(34) Mannequin, C.; Gonon, P.; Vallée, C.; Latu-Romain, L.; Bsiesy, A.; Grampeix, H.; Salaün, A.; Jousseaume, V. Stress-Induced Leakage Current and Trap Generation in HfO_2 Thin Films. *J. Appl. Phys.* **2012**, *112*, 074103-1−074103-9.
(35) Harrell, W. R.; Frey, J. Observation of Poole-Frenkel Effect Saturation in SiO_2 and Other Insulating Films. *Thin Solid Films* **1999**, *352*, 195−204.
(36) De Salvo, B.; Ghibaudo, G.; Pananakakis, G.; Guillaumot, B.; Reimbold, G. A General Bulk-Limited Transport Analysis of a 10 nm-Thick Oxide Stress-Induced Leakage Current. *Solid-State Electron.* **2000**, *44*, 895−903.
(37) Lampert, M. A.; Mark, P. *Current Injection in Solids*; Academic Press: New York and London, 1970.
(38) Paskaleva, A.; Lemberger, M.; Bauer, A. J.; Frey, L. Implication of Oxygen Vacancies on Current Conduction Mechanisms in TiN/$Zr_{1-x}Al_xO_2$/TiN Metal-Insulator-Metal Structures. *J. Appl. Phys.* **2011**, *109*, 076101-1−076101-3.
(39) Park, T. J.; Kim, J. H.; Jang, J. H.; Lee, C. K.; Na, K. D.; Lee, S. Y.; Jung, H. S.; Kim, M.; Han, S.; Hwang, C. S. Reduction of Electrical Defects in Atomic Layer Deposited HfO_2 Films by Al Doping. *Chem. Mater.* **2010**, *22*, 4175−4184.
(40) Boeske, T. *Crystalline Hafnia and Zirconia Based Dielectrics for Memory Applications*, Ph.D. Thesis; Technische Universitat Hamburg, Harburg, Germany, 2008.
(41) Quah, H. J.; Cheong, K. Y. Characterization of Ultrathin Al_2O_3 Gate Oxide Deposited by RF-Magnetron Sputtering on Gallium Nitride Epilayer on Sapphire Substrate. *Mater. Chem. Phys.* **2014**, *148*, 592−604.
(42) Kim, T. H.; Park, I. H.; Lee, J. D.; Shin, H. C.; Park, B. G. Electron Trap Density Distribution of Si-Rich Silicon Nitride Extracted Using the Modified Negative Charge Decay Model of Silicon-Oxide-Nitride-Oxide-Silicon Structure at Elevated Temperatures. *Appl. Phys. Lett.* **2006**, *89*, 063508-1−063508-3.
(43) Pan, T. M.; Chen, F. H.; Jung, J. S. Structural and Electrical Characteristics of High-*k* Tb_2O_3 and Tb_2TiO_5 Charge Trapping Layers for Nonvolatile Memory Applications. *J. Appl. Phys.* **2010**, *108*, 074501-1−074501-5.
(44) Di Maria, D. J. Determination of Insulator Bulk Trapped Charge Densities and Centroids from Photocurrent-Voltage Charactersitcs of MOS Structures. *J. Appl. Phys.* **1976**, *47*, 4073−4077.

DOI: 10.1021/acsami.5b03071
ACS Appl. Mater. Interfaces 2015, 7, 17032−17043